Proceedings of the ASME 2017 Pressure Vessels and Piping Conference
PVP2017
July 16-20, 2017, Waikoloa, Hawaii, United States

PVP2017-65156

FUZZY SEMI-ACTIVE CONTROL OF MULTI-DEGREE-OF-FREEDOM STRUCTURE USING MAGNETORHEOLOGICAL ELASTOMERS

Nguyen Xuan Bao
Graduate School of Natural Science and Technology, Kanazawa University
Kanazawa, Ishikawa 920-1192 JAPAN

Toshihiko Komatsuzaki
Institute of Science and Engineering, Kanazawa University
Kanazawa, Ishikawa 920-1192 JAPAN

Yoshio Iwata
Institute of Science and Engineering, Kanazawa University
Kanazawa, Ishikawa 920-1192 JAPAN

Haruhiko Asanuma
Institute of Science and Engineering, Kanazawa University
Kanazawa, Ishikawa 920-1192 JAPAN

ABSTRACT

Magnetorheological elastomer (MRE), used in semi-active control, has recently emerged as a smart material that could potentially improve traditional systems in controlling structural vibrations. This study considers two main issues concerning the application of an MRE. The first issue is the modelling and identification of the viscoelastic property, and the second is the formulation of an effective control strategy based on the fuzzy logic system. Firstly, a nonlinear dynamic MRE model was developed to simulate the dynamic behavior of MRE. In this model, the viscoelastic force of the material as an output was calculated from displacement, frequency, and magnetic flux density as inputs. The MRE model consisted of three components including the viscoelasticity of host elastomer, magnetic field-induced property, and interfacial slippage that were modeled by analogy with a standard linear solid model (Zener model), a stiffness variable spring, and a smooth Coulomb friction, respectively. The model parameters were identified by manipulating two sets of data that were measured by changing applied electric current and harmonic excitation frequency. A good agreement was obtained between numerical and experimental results. The proposed model offers a beneficial solution to numerically investigate vibration control strategies. Secondly, a fuzzy semi-active controller was designed for seismic protection of building with an MRE-based isolator. The control strategy was designed to determine the command applied current. The proposed strategy is fully adequate to the nonlinearity of the isolator and works independently with the building structure. The efficiency of the proposed fuzzy semi-active controller was investigated numerically by MATLAB simulations, whose performance was compared with that of passive systems and a system with traditional semi-active controller. Numerical results show that the developed fuzzy semi-active controller not only mitigates the responses of both the base floor and the superstructure, but also has an ability to control structural vibrations adaptively to the different intensity ground motions.

1. INTRODUCTION

Magnetorheological (MR) material is a class of smart materials whose rheological property can be adjusted by controlling an applied external magnetic field. MR fluid (MRF) is a classical MR material that is well known in various fields, such as automotive industry and civil engineering. The MR elastomer (MRE) has become a new kind of MR material that could potentially overcome the disadvantages of the fluid, such as the particle deposition and the sealing problems.

In order to design MRE-based isolator systems for various technical applications, numerical model should be developed that expresses viscoelastic behavior of the material and predicts operation processes of MRE-based isolator. However, MRE-based system is a nonlinear system in both shear modulus and damping properties. Furthermore, the properties depend on magnetic flux density, frequency excitation, and amplitude excitation. Therefore, modeling of the MRE properties is a big challenge, particularly in vibration control technology. Recently,

MRE modeling has been considered from different viewpoints. R. Li et al. [1] proposed a micromechanics-based viscoelastic model with chain structure, by which they predicted magnetic-field-dependent dynamic shear stiffness and damping of MRE. W. H. Li et al. [2] developed four-parameter viscoelastic model for MRE. In this model, a spring element is in parallel with the standard Kelvin-Voigt model, by which viscoelastic properties of MRE under harmonic loadings are predicted. However, the strain amplitude was not above 10% and frequency was less than 10 Hz. Eem et al. [3] developed a nonlinear dynamic model that combined the Ramber-Osgood model and Maxwell model. This model uses simple algebraic equations to represent hysteretic nonlinearity. However, its parameters are independent of displacement and frequency. Use of Bouc-Wen (1976) model to represent the nonlinear hysteresis is well known in MRF model. The Bouc-Wen model is well acceptable in MRE model in recent years [4]. However, one of the big problems in Bouc-Wen model is a need for identification of its seven parameters. M. Norouzi et al. [5] proposed a modified Kelvin-Voigt viscoelastic model for MRE-based isolator, whose coefficients are calculated by nonlinear regression technique. This model only works effectively in low-frequency ranges.

The MRE-based isolator is one of the semi-active devices, which requires an efficient controller. Because of nonlinearity in the model, not many control algorithms exist that could effectively operate MRE devices. The on-off algorithm has been widely used [6]. Opie et al. [7] developed a clipped-optimal controller for an MRE-based isolator. M. Behrooz et al. [8] used Lyapunov algorithm in seismic control. Du et al. [9] applied a sub-optimal H-∞ strategy to suppress the vibration of a vehicle seat suspension. In these algorithms, the command applied current has only two options: either zero or a maximum value. Consequently, fast switching produces periodical acceleration and jerk peaks that result in negative effects on the quality of structures.

In this study, the fuzzy semi-active controller was developed for switching MRE property. Firstly, the dynamic viscoelastic model of MRE was developed to simulate the dynamic behavior of MRE. The developed model worked efficiently in wide range of frequency and amplitude. We also proposed a procedure that could determine the parameters in the model. Secondly, a fuzzy semi-active controller was designed for seismic protection of building with an MRE-based isolator. The developed controller was successful in overcoming the disadvantages of conventional semi-active controller.

2. DYNAMIC MODEL OF MRE

2.1 Dynamic Model of MRE

In order to capture the dynamic properties of the MRE, the MRE was modeled by a dynamic system, as shown in Fig. 1. The model consisted of a standard linear solid model (Zener model), a stiffness variable spring, and a smooth Coulomb friction. We introduced the standard linear solid model in order to simulate

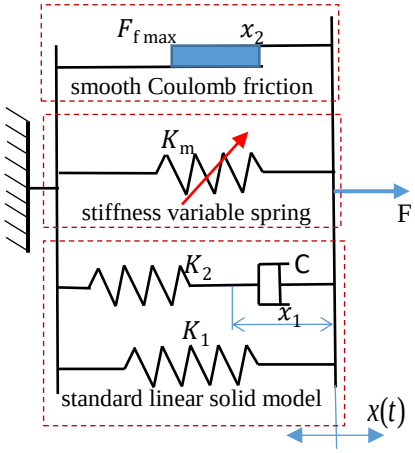

Fig. 1 MRE component model.

the viscoelasticity of the host MRE. The relationship between force and displacement can be described as follows:

$$F_1 = K_1 x, \quad (1)$$

$$F_2 = C\dot{x}_1, \quad (2)$$

$$F_2 = K_2(x - x_1), \quad (3)$$

$$F_v = F_1 + F_2, \quad (4)$$

$$\Delta E_v = \frac{\pi\omega C}{1+(\omega/\omega_v)^2} x_0^2, \quad (5)$$

where K_1 is the stiffness of spring element which corresponds to the stiffness of the host MRE, K_2 is the viscous stiffness, C and x_1 are the damping and displacement of the damping, respectively. F_1 and F_2 are the elastic force and the viscous force, F_v and x correspond to the viscoelastic force and displacement of the component, ΔE_v is the energy loss per cycle caused by the viscoelastic force, $\omega_v = K_2/C$ is the characteristic frequency, and ω is the excitation frequency.

When MRE is exposed to a magnetic field, the embedded ferromagnetic particles are magnetized. The magnetic force, F_m, is assumed to be expressed as,

$$F_m = K_m x, \quad (6)$$

$$\Delta E_m = 0, \quad (7)$$

where K_m is the variable stiffness, ΔE_m is the energy loss per cycle caused by the magnetic force.

The friction can be modeled as a smooth Coulomb friction force [10] as,

$$F_f = F_{fs} + \frac{x - x_s}{x_2(1 - sign(\dot{x})\alpha) + sign(\dot{x})(x - x_s))}(F_{f\max} - sign(\dot{x})F_{fs}), \quad (8)$$

$$\Delta E_f = 2F_{f\max}\left(2x_0 - x_2(1+\alpha)^2 \ln\frac{x_2(1+\alpha)+2x_0}{x_2(1+\alpha)}\right), \quad (9)$$

where $F_{f\,max}$ is the maximum friction force, x_2 is the displacement needed for the friction force to reach $F_{f\,max}/2$, ΔE_f is the energy loss per cycle caused by the friction. F_{fs} and x_s are a reference friction force and a displacement relative to static equilibrium, whose values are updated once. $\alpha = F_{fs}/F_{fmax}$ is an auxiliary quantity ranging from -1 to 1, and $sign(\dot{x})$ denotes the signum function of displacement rate.

Since three forces, generated in the standard linear solid model, in the stiffness variable spring, and in smooth Coulomb friction element, are connected in parallel, the total force, F, and the loss energy per cycle, ΔE , can be expressed as follows,

$$F = F_v + F_m + F_f, \tag{10}$$

$$\Delta E = \Delta E_v + \Delta E_f. \tag{11}$$

Table 1 Parameters defined for different applied current

	0 A	2 A	4 A	6 A
K_1 [N/mm]	13	13	13	13
K_2 [N/mm]	9	9	9	9
C [N.s/mm]	0.035	0.035	0.035	0.035
K_m [N/mm]	0	6.5	11	11.5
F_{fmax} [N]	2.4	6.5	9.5	10
x_2 [mm]	0.09	0.09	0.09	0.09

2.2 Experimental setup

Fabricated MRE samples consisted of Room Temperature Vulcanization (RTV) silicone rubber (high-strength condensation-cure type, Shin-etsu KE1416), silicone oil, and iron particles (BASF SG-BH) with average diameter of 20 μm. The materials were then placed in a mixer in order for the mixture to become homogenous. The mixture was placed in a copper mold and compressed to remove air bubbles. Finally, the mixture was cured under a magnetic field of 0.5 T at room temperature for 24 hours. An anisotropic elastomer sample was formed in square cuboids of sides 25 mm, thickness 10 mm, and iron content of 40 vol%.

The measurement setup is shown in Fig. 2. In this system, two MREs were placed between the iron cores of an electromagnet. An electromagnet consisted of an iron core and a magnetic coil as shown in Fig. 2b. A wire of diameter 1 mm was used to wind the coil in 800 turns. Two MREs were placed in gaps between upper and lower cores of electromagnet. In these gaps, a magnetic flux density is varied from 0 mT to 326 mT responding to a current changed from 0 A to 6 A, respectively. While the lower core was installed on a base exposed to excitation, the upper core was fixed along with a load sensor. The base was excited by a shaker whose excitation signal was supplied by a signal generator and a power amplifier. The displacement of the base and upper core's force were measured by using a laser displacement sensor and a load sensor, respectively. The force-displacement response was processed by a Fast Fourier Transform (FFT) spectrum analyzer. A direct current (DC) power supply provided adjustable direct current to a magnetic coil. In dynamic tests, numerous experiments were conducted for various harmonic inputs. The excitation frequency was adjusted from 1 Hz to 30 Hz, excitation amplitude was changed from 0.4 mm to 1.4 mm, and applied current was driven from 0A to 6A (magnetic flux density was adjusted from 0 mT to 326 mT).

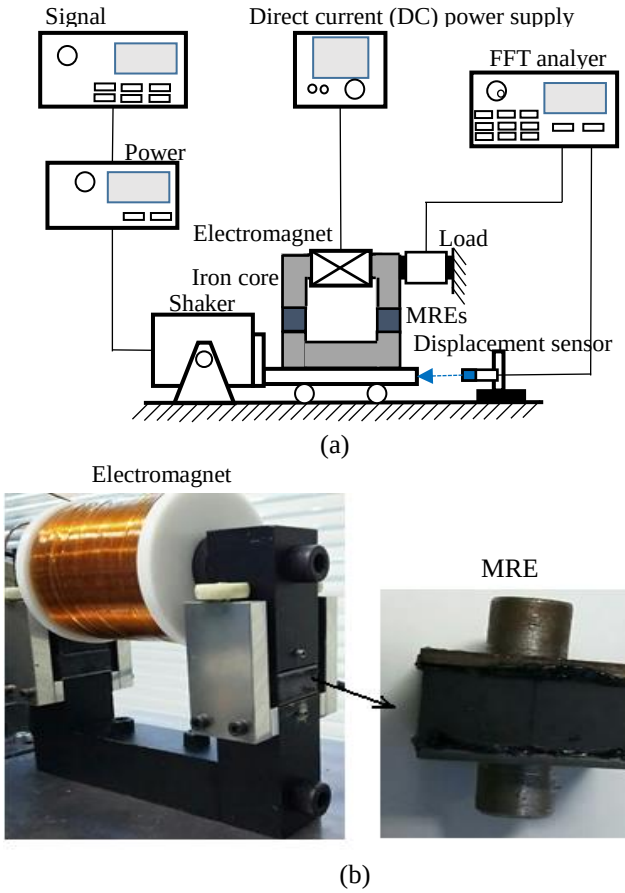

Fig. 2 MRE viscoelastic property measurement: (a) schematic and (b) photograph.

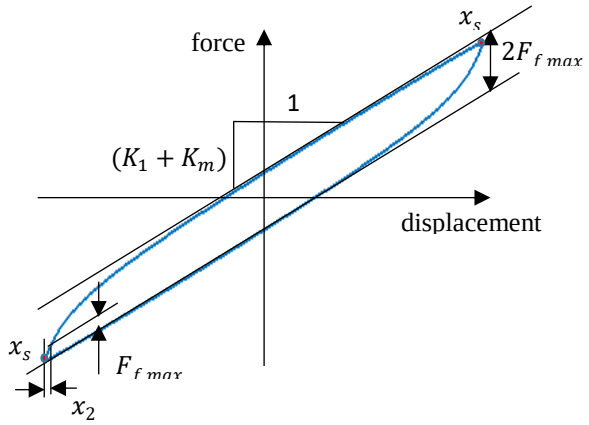

Fig. 3 Definitions of the model parameters K_1, K_m, $F_{f\,max}$, and x_2.

2.3 Determination of model parameters

The parameters were determined according to the following procedure.

Step 1: Determination of the model parameters $K_1, K_m, F_{f\,max}$, and x_2.

The displacement amplitude, $x_0 = 1$ mm, and excitation frequency, f=1 Hz, were chosen for experiment. The force-displacement curve is shown in Fig. 3. In the case of low excitation frequency, the viscous effects, which are modeled by Eqs. (2) and (5), become extremely small and they can be neglected ($F_2 \approx 0, E_v \approx 0$). When displacement becomes $x \gg x_s$ or $x \ll x_s$ (x_s is the static equilibrium), the friction force, represented by Eq. (8), becomes maximum ($F_f = F_{max}$). The total force and loss factor per cycle in Eqs. (10) and (11) are rewritten as,

$$F = (K_1 + K_m)x + F_{f\,\max}, \tag{12}$$

$$\Delta E = \Delta E_f, \tag{13}$$

where $F(x)$ is the force determined by measured force-displacement loop, ΔE is the loss energy per cycle determined by the area enclosed by the loop, K_1 is the nominal stiffness of MRE without magnetic field, and K_m is the increment stiffness when the electric current is applied. Consequently, K_1, K_m, F_{fmax}, and ΔE_f were calculated, where x_2 was used to determine the rate at which the friction force developed relative to the displacement. The parameters are illustrated in Fig. 3.

Step 2: Determination of the viscosity parameters, K_2, C

Under the constant displacement amplitude $x_0 = 1$ mm, frequency was set at f=2, 3, 4,…, 30 Hz. From the experiments, the maximum loss energy, $\Delta E_{max}(\omega)$, was used for determining model parameters. From Eq. (9), the friction loss energy (ΔE_f) is found to be independent of excitation frequency. The viscous loss energy, modeled by Eq. (5), is dependent on frequency and reaches maximum at characteristic frequency $\omega = K_2/C$,

$$\Delta E_{v\,max}(\omega) = \frac{1}{2}\pi\omega C x_0^2 = \Delta E_{max}(\omega) - \Delta E_f, \tag{14}$$

where $\Delta E_{max}(\omega)$ and $\omega = K_2/C$ are the maximum loss energy and the characteristic frequency determined by experimental results. ΔE_f is determined by Eq. (13) in step 1. The model viscosity parameters, K_2 and C were then identified.

Step 3: Redo step 1 and step 2 for different applied currents.

The identified parameters are show in Table 1. From the table, the model parameters such as K_e, K_v, C, and x_2 were found to change insignificantly by applied currents. On the other hand, the parameters, K_m, and $F_{f\,max}$ increased significantly by increasing current. From the values in Table 1, K_m and $F_{f\,max}$ were approximated by the following continuous function.

$K_m = -0.38I^2 + 4.25I$, $F_{f\,max} = -0.24I^2 + 2.75I + 2.4$
$I \in [0,6]$

In conclusion, the model parameters were calculated, as listed in Table 2.

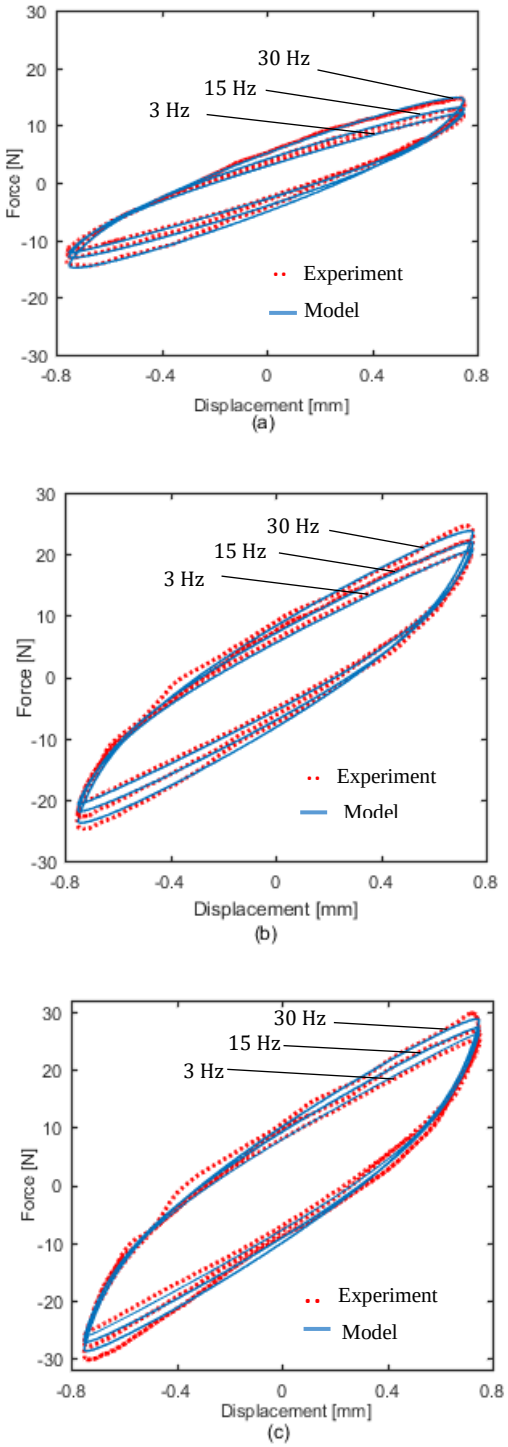

Fig. 4 Force-displacement response under different frequencies with excitation amplitude $x_0 = 0.75\,mm$: (a) I= 0 A (0 mT), (b) I= 2 A (218 mT), and (c) I= 4 A (267 mT).

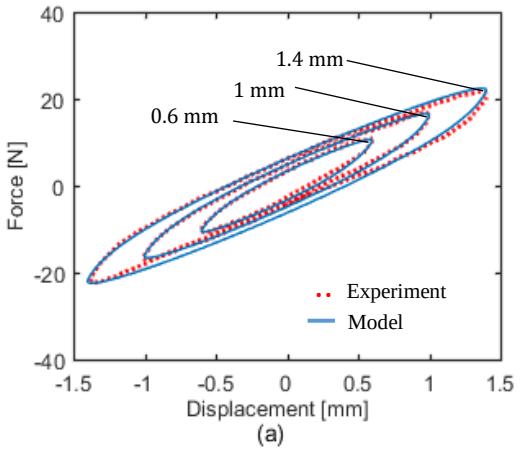

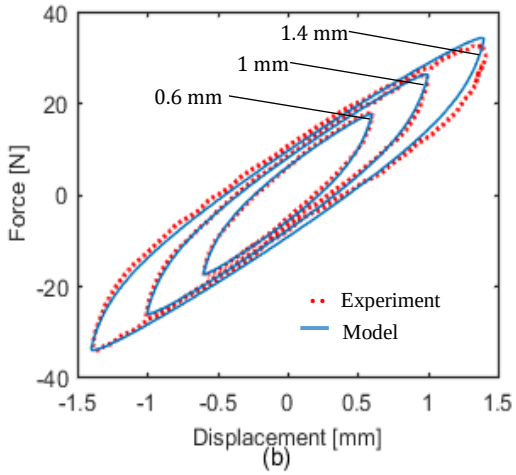

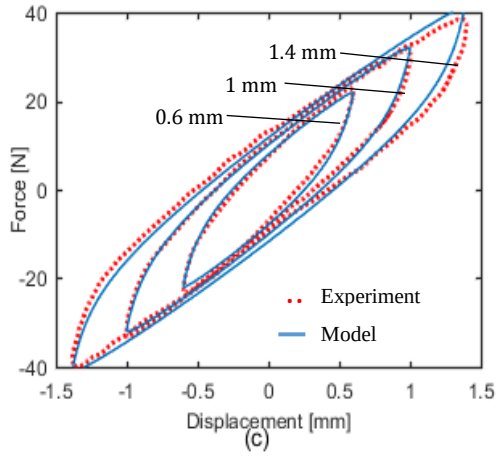

Fig. 5 Force-displacement response under different amplitude levels with excitation frequency f =15 Hz: (a) I= 0 A (0 mT), (b) I= 2 A (218 mT), and (c) I= 4 A (267 mT).

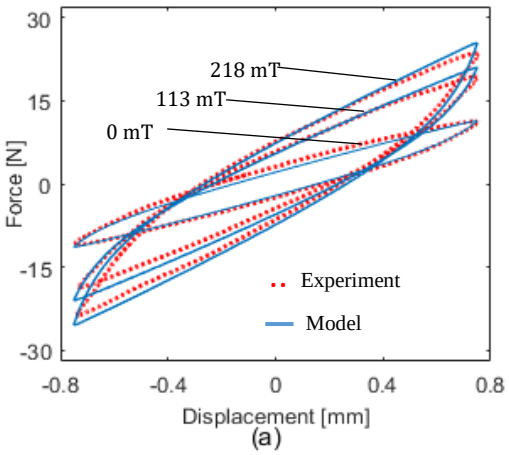

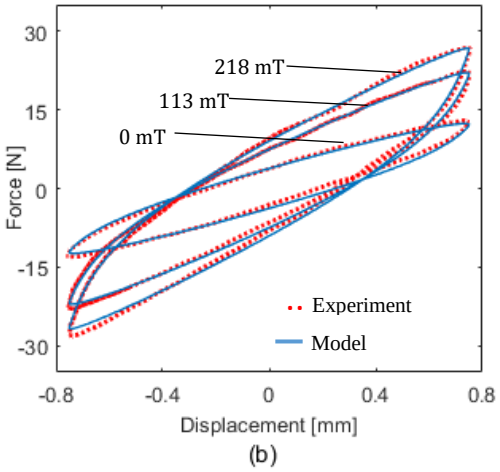

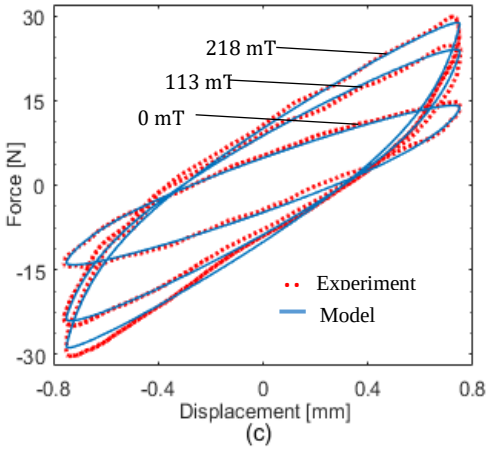

Fig. 6 Force-displacement response under different levels of applied current with excitation amplitude $x_0 = 0.75\ mm$: (a) f = 1 Hz, (b) f=15 Hz, and (c) f =30 Hz.

Table 2 Parameter for the proposed MRE model

Stiffness (K_1)	13 Nmm^{-1}
Stiffness (K_2)	10 Nmm^{-1}
Viscous damping (C)	0.035 Nsm^{-1}
Friction displacement (x_2)	0.09 mm
Maximum friction force ($F_{f\,max}$)	$F_{f\,max} = -0.24I^2 + 2.75I + 2.4$
Variable stiffness (K_m)	$K_m = -0.38I^2 + 4.25I$
Applied current (I)	$I \in [0,6]$ Ampere

2.4. Comparison of simulation and experimental results

The proposed MRE model and relevant simulation results were compared with experimental results obtained by a harmonic excitation. Three levels for displacement, three levels for input frequency, and four levels for magnetic field were arranged.

2.4.1 Frequency dependency

A displacement amplitude, $x_0 = 0.75$ mm, was set at excitation frequencies: f = 3, 15, and 30 Hz. The measurements were performed in three levels of the magnetic field: 0 mT (0 A), 113 mT (2 A), and 218 mT (4 A). The force-displacement loops are shown in Fig. 4. The overall agreement between measured and simulated loops was found. The loops tended to become elliptic as the frequency increased. The gradient of the main axis and the area of hysteresis loops became large as the external magnetic field increased. The smooth Coulomb friction model is adaptable for representing the rate-dependence of the force-displacement relationship.

2.4.2 Amplitude dependency

Under a harmonic excitation with frequency f=15 Hz, three displacement amplitudes were provided: $x_0 =$ 0.4, 0.8, and 1.4 mm. The measurements and simulations were performed for three levels of magnetic field strength: 0 mT (0 A), 113 mT (2 A), and 218 mT (4 A). The force-displacement loops are compared in Fig. 5. The force-displacement loops obtained by the numerical model agreed well with experimental result. The slopes of hysteresis loops decreased with increase in amplitude and this trend is the same for all values of magnetic fields.

2.4.3 Magnetic field dependency

Under the displacement amplitude of $x_0 = 0.75$ mm, three levels of magnetic field were applied to the isolator: 0 mT (A), 113 mT (2 A), and 218 mT (4 A). The measurements and simulations were performed for three different excitation frequencies: 3 Hz, 15 Hz, and 30 Hz. The force-displacement loops are shown in Fig. 6. A good agreement between measured and simulated loops was found. The loops tended to become elliptic as the magnetic flux density increases. The difference between measured and simulated loops showed the same degree of error in different levels of magnetic flux density.

3. SEMI-ACTIVE CONTROL STRATEGY

We consider a seismically excited structure controlled by switching viscoelastic property of an MRE. The equation of motion can be written as follows,

$$M\ddot{x} + C\dot{x} + Kx = \Lambda f_{MRE} - M\Gamma\ddot{x}_g, \tag{15}$$

In Eq. (15), M, C, and K represent $(n \times n)$ mass, damping, and stiffness matrices, respectively; x is the vector of the displacements of the floors relative to the ground; f_{MRE} is the control force generated by a MRE-based isolator; $\ddot{x}_g$ is ground acceleration; Λ is the matrix determined by the placement of control devices; Γ is the column vector of ones. This equation can be written in state space form as follows,

$$\dot{z} = Az + Bf_{MRE} + E\ddot{x}_g, \tag{16}$$

$$y = Cz + Df_{MRE}, \tag{17}$$

where z is the state vector; y is the vector of measured outputs.

3.1 Semi-active control

For the present application, a Lyapunov-based control strategy is used; it is robust, it can minimize transferred energy to the structure, and it can be used for both linear and nonlinear systems [11]. The Lyapunov function can be expressed as,

$$V = \frac{1}{2}x^T Kx + \frac{1}{2}\dot{x}^T M\dot{x}. \tag{18}$$

The derivative of the Lyapunov function associated with (Eq. 15) can be derived as follows,

$$\begin{aligned}\dot{V} &= x^T K\dot{x} + \dot{x}^T M\ddot{x} \\ &= x^T K\dot{x} + \dot{x}^T(-C\ddot{x} - Kx - M\Gamma\ddot{x}_g + \Lambda f_{MRE}).\end{aligned} \tag{19}$$

The control input current, which is defined by the following equation with respect to the measured force, can minimize $\dot{V}$,

$$I_{control} = I_{\max} H(-\dot{x}^T \Lambda f_{MRE}). \tag{20}$$

where H is the Heaviside step function. In this algorithm, the command applied current has the choice of being either zero or maximum value. The fast switching of the on-off algorithm causes high acceleration and jerk peaks periodically, thus leading to the degeneration of the overall system quality. The problem can be resolved using fuzzy logic to soften the fast switching action of the on-off control.

3.2 Fuzzy semi-active control

The fuzzy logic controller is designed to determine the command applied current of MRE-based isolator according to the velocity and displacement of the isolator. The MRE regulates the viscoelastic force according to the input applied current. The

block diagram of the system for the developed controller is shown in Fig. 7.

The displacement and velocity of the structure are selected as two input variables (Fig. 8), and command applied current is employed as a single output variable (Fig. 9). The definitions of the membership function of input variables are as follows: negative large (NL); negative medium (NM); negative small (NS); zero (ZE); positive small (PS); positive medium (PM); positive large (PL). As the control output, applied current is as follow: zero (ZE); small (S); medium (M); large (L); and very large (VL). The membership functions are structured in the shape of a triangular with Mamdani-type inference system; the center of gravity method is used for de-fuzzification. The rules are based on the skyhook on-off algorithm.

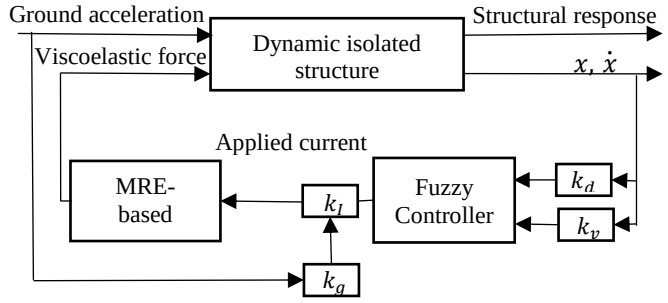

Fig. 7 Diagram of fuzzy control system

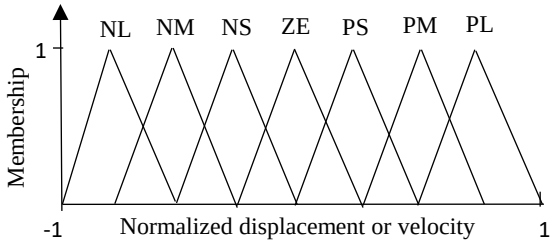

Fig. 8 Input membership functions

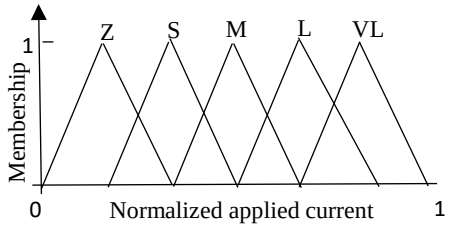

Fig. 9 Output membership functions

Table 3 Fuzzy inference rule

$\dot{x}$ \ x	NL	NM	NS	ZE	PS	PM	PL
NL	VL	VL	L	L	M	S	ZE
NM	VL	VL	L	M	S	ZE	S
NS	VL	L	M	S	ZE	S	M
ZE	L	M	S	ZE	S	M	L
PS	M	S	ZE	S	M	L	VL
PM	S	ZE	S	M	L	VL	VL
PL	ZE	S	M	L	L	VL	VL

The fuzzification factors used to convert the inputs into fuzzy variables are defined as k_d and k_v, for displacement and velocity, respectively. The de-fuzzification factor used to convert the output was k_I. Since the applied current is driven from 0 A to 5 A, the value of de-fuzzification factor is equal to the maximum value of applied current ($k_I = 5$). From the best results among many cases studied, k_I seems to be strongly related to ground acceleration.

3.3 Numerical example

To evaluate the performance of the proposed algorithm along with the use of MRE-based isolator, we considered the three-story building structure model as shown in Fig. 10. The MRE-based isolator is rigidly connected between the ground and the first floor of the structure.

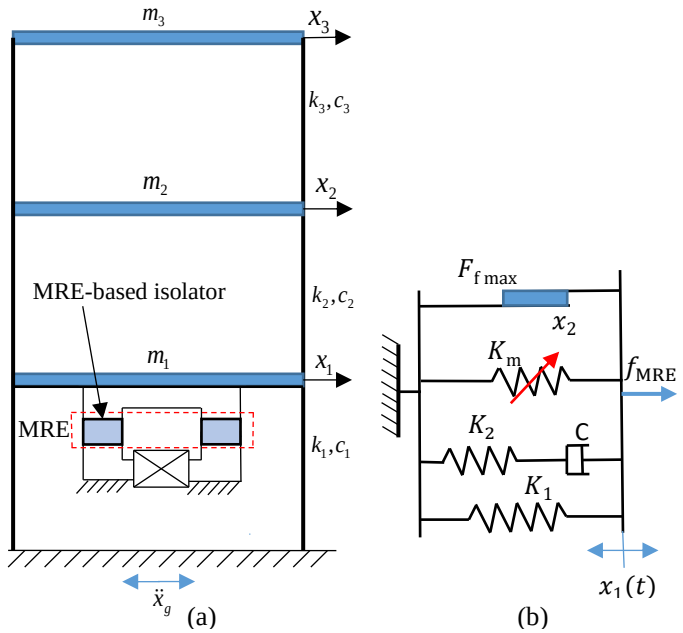

Fig. 10 Schematic diagram of the MRE implementation: (a) a three-story building structure employs an MRE-based isolator, and (b) the MRE-based isolator.

The system matrices of a three-story shear building are,

$$M = \begin{bmatrix} 10 & 0 & 0 \\ 0 & 10 & 0 \\ 0 & 0 & 10 \end{bmatrix} kg,$$

$$C = \begin{bmatrix} 4 & -2 & 0 \\ -2 & 4 & -2 \\ 0 & -2 & 2 \end{bmatrix} \frac{N.\sec}{m},$$

$$K = \begin{bmatrix} 20 & -10 & 0 \\ -10 & 20 & -10 \\ 0 & -10 & 20 \end{bmatrix} \frac{N}{mm}. \quad (21)$$

The MRE-based isolator was rigidly fixed between the ground and the first floor of the structure. The test structure was excited by the El Centro and Kobe earthquakes. Because the system under consideration was a scaled model, the recorded earthquake signal were also scaled as appropriate.

The displacement responses obtained at the third floor are show in Fig. 11. The performances of the Lyapunov semi-active and the Fuzzy semi-active controllers are compared for the El Centro and Kobe earthquakes. As seen from the figure, the third floor response was significantly reduced by both controllers in comparison to the case without the MRE-based isolator. The maximum displacement and acceleration distributed over the structure is schematically shown in Figs. 12 and 13. The harmful vibration in the structure was satisfactorily reduced by the controllers. These figures show that the minimum displacement and acceleration for each story were obtained for Fuzzy semi-active strategy.

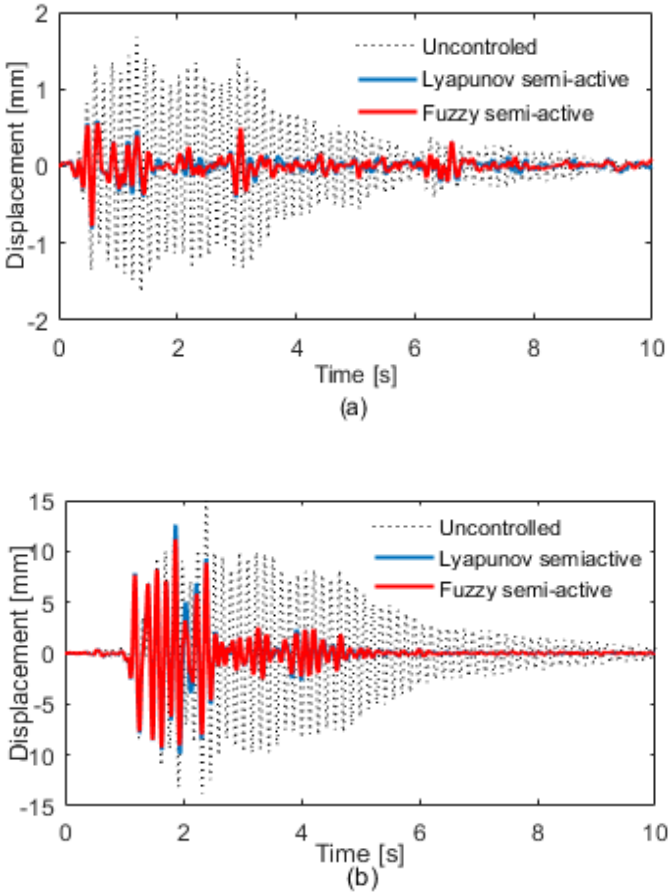

Fig. 11 Comparision of Controlled and Uncontrolled displacement responses in the third floor: (a) El Centrol earthquake, and (b) Kobe earthquake.

Fig. 14 shows the command applied current supplied to the MRE-based isolator while the system was excited by the El Centro and Kobe earthquake waves. The command applied current for the isolator with Lyapunov strategy switched alternatively: either zero or maximum value (5A). However, the command applied current for the isolator with Fuzzy strategy was changed continuously between two extremes. In the case of large displacement, it is known from Figs. 11 and 14 that the applied current for both isolators varied in the same on-off manner. In the case of small displacement, the Lyapunov semi-active controller produced maximum applied current around equilibrium. However, the fuzzy semi-active controller produced a sufficient applied current.

The RMS and maximum values of the third floor response are listed in Tables 4 and 5. The values in parentheses represent the ratio of the values to those obtained for the uncontrolled case without MRE-based isolator. The RMS ratios of the displacement response when using the fuzzy semi-active control decreased significantly to 0.21 and 0.46 for the El Centro and Kobe earthquake, respectively. In addition, the acceleration RMS values also decreased in the case of the fuzzy semi-active control. The maximum displacement and acceleration responses when using the fuzzy semi-active control were reduced significantly. The maximum ratios of the displacement response in the fuzzy semi-active control decreased to 0.34 and 0.75 for respective earthquakes. The overall performance of the structure that used the fuzzy semi-active control surpassed that of the passive systems. The fuzzy semi-active system performed slightly better than the Lyapunov semi-active structure.

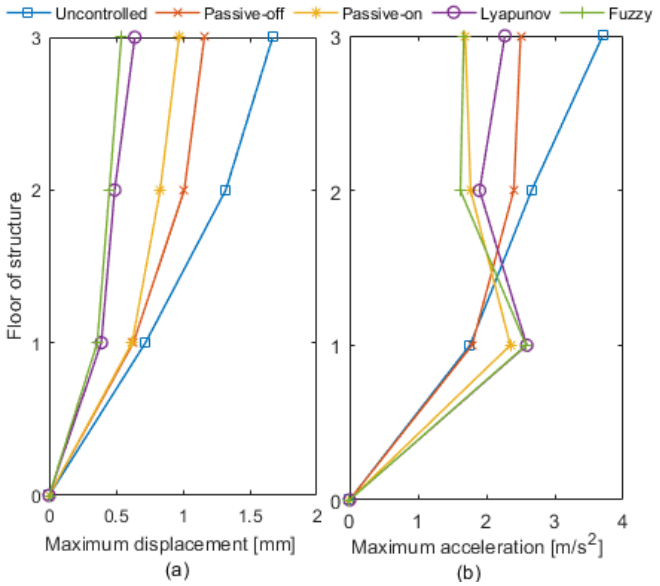

Fig. 12 Maximum displacement and acceleration for each floor of structure under El Centro earthquake: (a) maximum displacement, and (b) maximum acceleration.

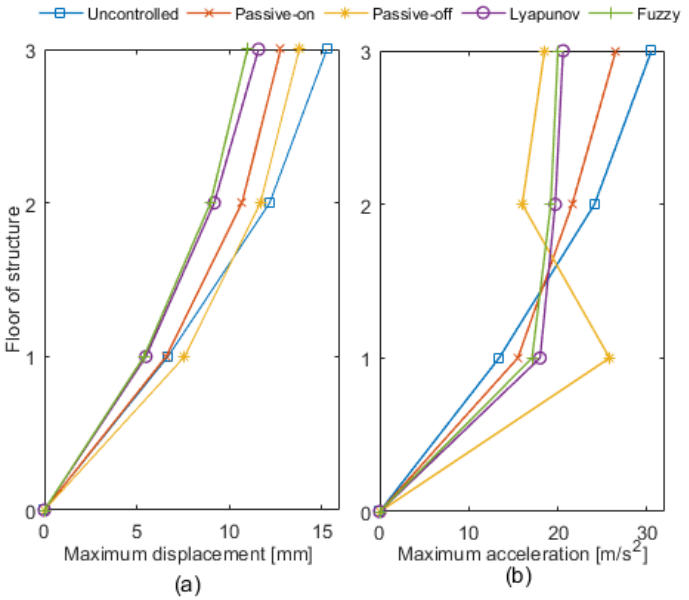

Fig. 13 Maximum displacement and acceleration for each floor of structure under Kobe earthquake: (a) maximum displacement, and (b) maximum acceleration.

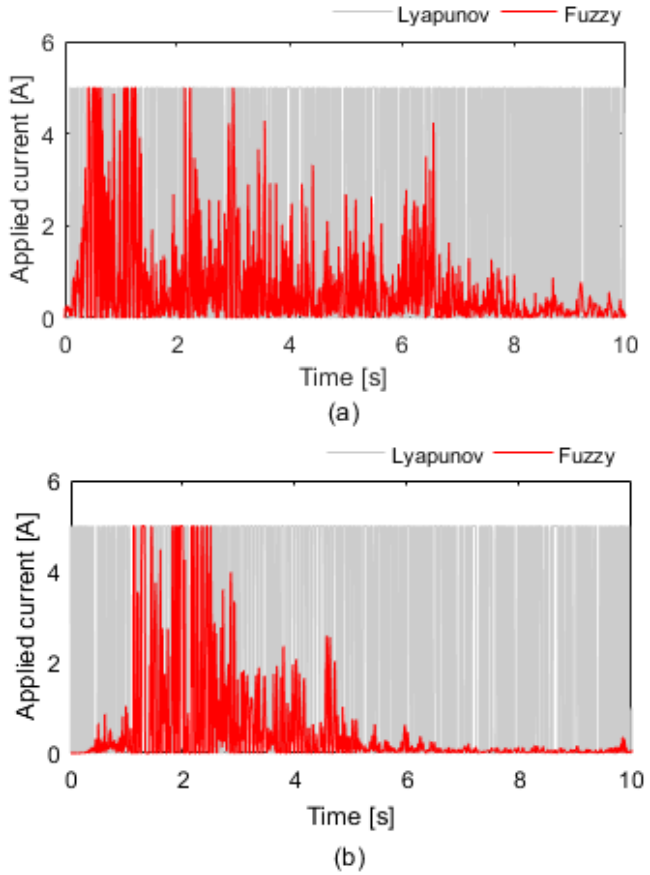

Fig. 14 Comparision of applied current for MRE-based isolator: (a) El Centro earthquake, and (b) Kobe earthquake.

Table 4 Evaluated performance indices in third floor due to El Centrol earthquake.

Control strategy	RMS disp. (mm)	Max. disp. (mm)	RMS acc. (ms^{-2})	Max. acc. (ms^{-2})
Uncontrol	0.46(1)	1.67(1)	0.91(1)	3.7(1)
Passive-off	0.23(0.5)	1.1(0.65)	0.42(0.46)	2.5(0.67)
Passive-on	0.18(0.39)	0.97(0.58)	0.23(0.25)	1.7(0.45)
Lyapunov	0.11(0.24)	0.59(0.35)	0.23(0.25)	1.8(0.48)
Fuzzy	0.1(0.21)	0.57(0.34)	0.22(0.24)	1.6(0.43)

Table 5 Evaluated performance indices in third floor due to Kobe earthquake.

Control strategy	RMS disp. (mm)	Max. disp. (mm)	RMS acc. (ms^{-2})	Max. acc. (ms^{-2})
Uncontrol	3.5(1)	15.3(1)	7.1(1)	30(1)
Passive-off	1.91(0.54)	12.8(0.83)	3.52(0.49)	26(0.86)
Passive-on	2.30 (0.65)	13.8(0.90)	3.58(0.50)	18(0.6)
Lyapunov	1.73(0.49)	12.6(0.82)	3.16(0.44)	20.8(0.69)
Fuzzy	1.62(0.46)	11.1(0.75)	3.19(0.45)	20.1(0.67)

4. CONCLUSIONS

In this study, the fuzzy semi-active control strategy was proposed for mitigating vibrations in the structure using the MRE-based isolator. The dynamic viscoelastic model of MRE-based isolator were presented, and a procedure to determine the six model parameters was introduced. The force-displacement relationship predicted by the model was almost consistent with the measured results. The viscoelastic force of MRE-based isolator was controlled by changing electric current applied to an electromagnet. The algorithm was developed with the aim of switching viscoelastic force smoother than the conventional Lyapunov algorithm. The results showed that the fuzzy semi-active controller provided better performance than its counterparts, not only by reducing responses, but also conserving the electrical energy of the device. Finally, the fuzzy semi-active control system using an MRE was found to be efficient for vibration control of three story building. The system has advantages over the conventional semi-active system.

ACKNOWLEDGMENTS

The work was supported by the Japan Society for the Promotion of Science (JSPS) KAKENHI, Grant-in-Aid for Scientific Research (B), Grant Number 15H03936.

REFERENCES

[1] Li, R. and Sun, L. Z., 2014, “Dynamic viscoelastic modeling of magnetorheological elastomers,” Acta Mech, 225, pp. 1347-1359.

[2] Li, W. H., Zhou, Y. and Tian, T. F., 2010, “Viscoelastic of MR elastomers under harmonic loading,” Rheol Acta, 49, pp. 733-740.

[3] Eem, S. H., Jung, H. J. and Koo, J. H., 2012, "Modeling of magneto-rheological elastomers for harmonic shear deformation," IEEE transactions on magnetics, 48 (11), pp. 3080-3083.

[4] Yang, J., Du, H., Li, W., Li, Y., Li, J., Sun, S. and Deng, H. X., 2013, "Experimental study and modeling of a novel magnetorheological elastomer isolator," Smart Materials and Structures, 22 (11), pp. 1-14.

[5] Norouzi, M., Alehashem, S. M. S., Vatandoost, H., Shahmardan, M. M., 2016, "A new approach for modeling of magnetorheological elastomers" Journal of Intelligent Material Systems and Structures, 27(8), pp. 1121-1135.

[6] Liao, G. J., Gong, X. L., Kang, C. J., and Xuan, S. H, 2011, "The design of an active–adaptive tuned vibration absorber based on magnetorheological elastomer and its vibration attenuation performance," Smart Material and Structures, 20(07), pp. 5015-5025.

[7] Opie, S. and Yim, W., 2010, "Design and control of a real-time variable modulus vibration isolator," Journal of Intelligent Material Systems and Structures, 22(2), pp. 113-125.

[8] Behrooz, M., Wang, X. and Gordaninejad, F., 2013, "Performance of a new magnetorheological elastomer isolator system," Smart Material and Structures. 23(04), 5014(8pp).

[9] Du, H., Li, W. and Zhang, N., 2011, "Semi-active variable stiffness vibration control of vehicle seat suspension using an MR elastomer isolator," Smart Material and Structures. 20(10), 5003 (10pp).

[10] Berg, M., 1998, "A non-linear rubber spring model for rail vehicle dynamics analysis," Vehicle System Dynamics, 30, pp. 197-212.

[11] Choi, K. M., Lee, H. J., Cho, S. W. and Lee, I. W., 2007, "Modifield energy dissipation algorithm for seismic structures using magnetorheological damper," KSCE Journal of Civil Engineering, 11 (2), pp. 121-126.